INTERNATIONAL SOCIETY FOR SOIL MECHANICS AND GEOTECHNICAL ENGINEERING



This paper was downloaded from the Online Library of the International Society for Soil Mechanics and Geotechnical Engineering (ISSMGE). The library is available here:

https://www.issmge.org/publications/online-library

This is an open-access database that archives thousands of papers published under the Auspices of the ISSMGE and maintained by the Innovation and Development Committee of ISSMGE.

Geotechnical properties of sandasphalt observed from field and laboratory tests

Caractéristiques du sable-bitumé observées lors d'essais 'in-situ' et en laboratoire

P. A. RUYGROK, Delft Soil Mechanics Laboratory, Netherlands R. J. TERMAAT, Rijkswaterstaat, The Hague, Netherlands E. O. F. CALLE, Delft Soil Mechanics Laboratory, Netherlands G. L. M. MULDERS, Bitumarin B.V., Zaltbommel, Netherlands

SYNOPSIS

Sandasphalt is a mixture of sand with 3 to 5 weight percents of bitumen. Its properties as a hydraulic filter and its resistance against erosion makes it a material for hydraulic engineering applications, more favourable than other materials. In order to get more acquainted to its properties as a hydraulic filter and its mechanical behaviour, an investigation has been set up. A special triaxial test procedure has been developed. The results were used in a modified Bishop stability analysis, which incorporates a visco-plastic stress strain relation. This analysis has been extended, in order to obtain a cheap but relatively rough tool for predicting time-dependent deformation of the slope, due to creep. A field test was set up in order to observe stability and deformation of a slope in practice.

INTRODUCTION

Sandasphalt is manufactured as a hot mixture of dry sand and 3 to 5 weightpercentage hitumen. Addition of bitumen leads to a grain coating of about 10 microns only. Moreover, as this coating smoothens the pore shape, it may be obvious that the permeability of (not overcompacted) sandasphalt is not significantly different from that of the constituent sand. The bonded character makes it a very attractive material for hydraulic engineering purposes. In most applications it serves as a filter material in dikes or dams with a sandy core. In dikes around a sandfill it is used for protection against eroding current (scour) and wave attack.

Applications have been described in a previous paper (Mulder, 1981). In addition to this paper, the present paper reports further progress of the investigation of filter properties and mechanical behaviour of sandasphalt. A model is presented for computational analysis of stability of slopes and rough prediction of creep deformation.

FILTER PROPERTIES

The void ratio of a normal sand with medium grainsize (0.15-0.4 mm) is in the range of 35-40%. Corresponding permeabilities range from $10^{-3}-10^{-5}$ m/s.

It has been argued in the introduction that permeabilities of a sandasphalt mix range in the same order. In order to investigate its suitability as a filter material, tests have been carried out to determine the critical hydraulic gradient. Figure 1 shows the test set up.

The shape of the sandasphalt sample is conical, in order to prevent it from being blown out of the apparatus at high pressures. No critical hydraulic gradient has been found during the tests, even at gradients up to 2000 percent. At these gradients, tensile cracks (following deformations in the order of 10-15 percent) initiated complete (break out) failure of the samples. Figure 2 shows the coefficients of permeability and the discharge q as functions of the hydraulic gradient i. It is remarkable to see that the permeability does not decrease as the hydraulic gradient increases. Figure 3 shows the results in the case of a sandlayer placed on top of the sandasphalt sample. An interesting phenomenon can be observed when the hydraulic head is increased. As the drop of hydraulic head over the sandlayer is limited by its critical gradient, the sandasphalt filter takes over the remaining head fall.

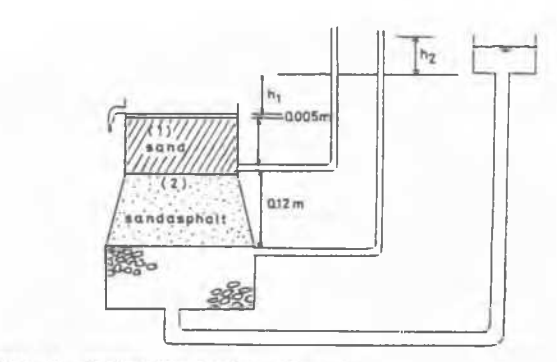


Fig. 1 Hydraulic test equipment

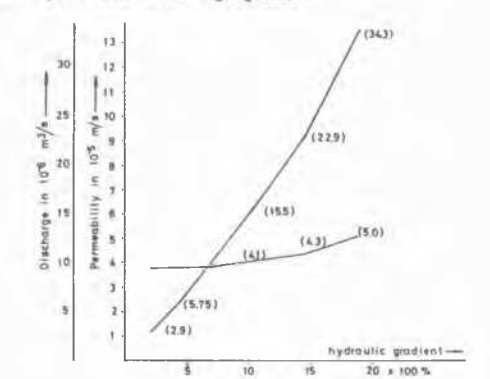


Fig. 2 Hydraulic characteristics

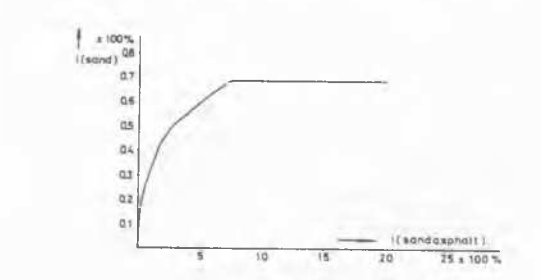


Fig. 3 Simultaneous hydraulic gradients

MECHANICAL CHARACTERISTICS OF LEAN SANDASPHALT

The rheologic model in fig. 1A was chosen out of a number of possibilities. It is based on the point of view that deformation resistance is built up partly in force transmitting branches with direct grain-to-grain contact (like in Cundall's BALL model) caused by local squeezing of coating. The other part of resistance is due to viscous flow at still intact or incompletely outsqueezed coating joints (viscous drag transmitting chains). Note that these joints are moreover capable to bear tensile stresses temporary and also will delay dilatancy trends.

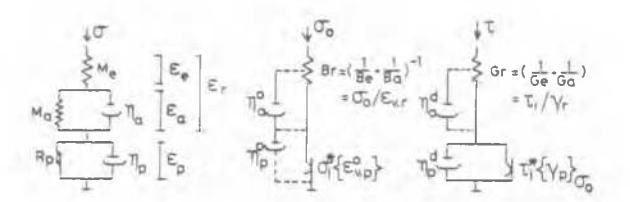


Fig. 4A General model Fig. 4B Simplified model

effective rather than material.

Fig. 4 Descriptive theological models

In fig. 1A elastic, visco-elastic and visco-plastic response occur in separate elements. The plastic resistance P is considered to originate from the direct grain contact interactions, but with reduced shear friction compared to a clean sand packing.

The viscosity of the adhesive bound coating is expected to be of larger magnitude compared to the case of free bituminous binder, and probably not isotropic. Therefore, the measured values should be considered as

In principle the model can be divided in a submodel for spherical stress (volumetric deformation) and deviatoric stress (shear).

The test procedure was based on fig. 1A and performed with a triaxial apparatus. In both the spherical stress and deviatoric test phase the plastic resistance functions and pseudo-elastic moduli are obtained from stress equilibrium (zero strain rate) at successive increased strains, followed by quick stress relieve to allow complete back creep.

Hence, the plastic and reversible strains are obtained. Note that during the deviatoric test phase the spherical stress level of the final stage of the spherical test phase should be maintained.

In the final test stage the deviatoric stress at constant strain rate attains a maximum indicating grain skeleton 'failure'. As virtually no visco-elastic contribution is involved, it applies (see fig. 4B)

$$\begin{split} &\tau_{(\text{max})} = \tau_{\text{i,f}}^{\star} + \eta_{p}^{d} \dot{\gamma}_{p'}, \\ &\text{where } \tau_{\text{i,f}}^{\star} = \text{'failure' limit, } \eta_{p}^{d} \text{ effective plastic shear} \\ &\text{viscosity, assuming } \dot{\gamma} = \dot{\gamma}_{p}. \end{split} \label{eq:tau_max}$$

To obtain the 'failure' limit the shear stress is decreased until zero strain rate occurs. Now the plastic shear viscosity is obtained according to formula (1). Between the successive deviatoric test-stages a creep cycle of spherical stress unloading and reloading is performed to observe possible changes in volumetric strain as a consequence of the preceeding plastic shear. These creep cycles are executed in multiple after the final stage of deviatoric testing in order to determine deformation-anisotropy effects at large plastic shear. In view of the observation that the relaxation time of viscoplastic shear far dominates the relaxation time of all other viscous phenomena (indicated in fig. 4B), the rheologic model may be simplified as presented in fig. 4B in case of monotonic (sustained) loading. However, a restriction of the model in fig. 4B is that it cannot represent specific phenomena like dilatancy or anisotropy. Laboratory-prepared test samples containing 3 weight % bitumen 80/100 were densified up to $\rho=1.6$ t/m² in a cylinder at mix temperature 130°C, and tested at 17,5 t 0,3°C. The spherical stress tests were performed up to nominal levels of 30, 50 and 70 kPa. The results, in relation to fig. 4B, are presented in

The results, in relation to fig. 4B, are presented in fig. 5.

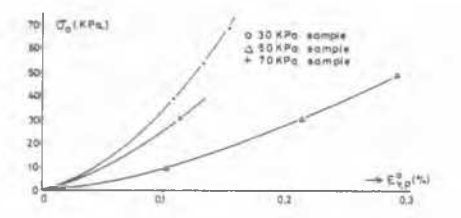


Fig. 5A Volumetric plastic resistance

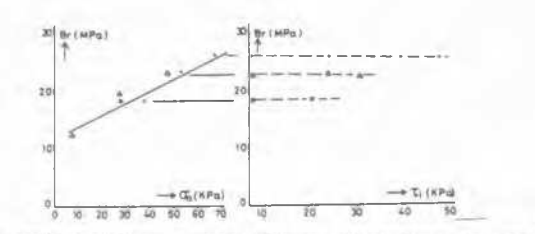


Fig. 5B Bulk modules Fig. 5C Br-dependence on shear

Fig. 5 Volumetric characteristics of lean sandasphalt

5A shows that the volumetric resistance is rather sensitive to small quality variance. In fig. 5B a practically linear dependence of bulk modulus Br (as defined above) on spherical stress level is present (note that contrary to fig. 5A the variance is quite modest). Results of the relieve of spherical stress in between the deviatoric test phases (thus at each of the levels 30, 50 and 70 kPA) are seen in fig. 5C.

Note that shear stress level (read: magnitude of plastic shear) has only minor influence on the bulk modulus. This permits to some extent (not too large shear) superposition of stress-strain relations from both test phases.

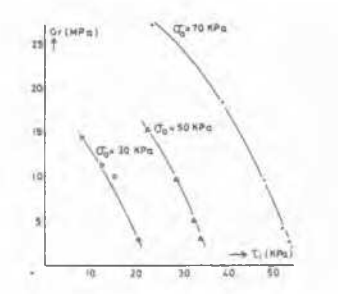


Fig. 6A Stress-dependence of shear modulus

In fig. 6A the stress-dependence of shear modulus Gr (as defined above) is demonstrated. The striking progressive decrease in Gr, related to plastic shear, in fact means that a significant fraction of shear strain is reversed in backcreep. Such may probably be attributed to tuck-up zones of the coating at incompletely squeezed coating-joints, relieving their elastic energy at unloading. The spherical stress (creep) cycles at failure strains, mentioned above, indicated in fact induced (partial) recovery of plastic shear, which to some extent supports the forecalled assumption.

Fig. 6B shows that the plastic shear resistance relation can be normalized satisfactory to the spherical stress

level (despite the variance noted in fig. 5A). The failure level may be expressed to represent an angle of internal friction of 35-37 degrees.

Fig. 6C presents the normalized plastic dilatancy relation. Drastic increase of dilatancy is observed only at the approach of 'failure' level.

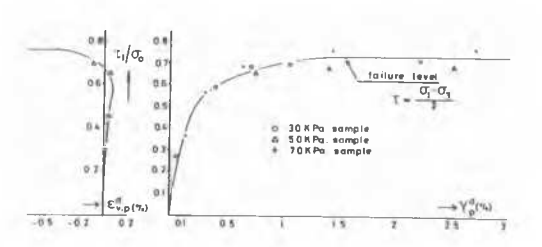


Fig. 6C Dilatancy Fig. 6B Plastic shear resistance relation

Fig. 6 Shear characteristics of lean sandasphalt

It was observed that the magnitude of the effective (plastic) viscosity depends somewhat on spherical stress level and shear strain rate.

As an average a value of $\eta_p = (2,2\pm0,5)\cdot 10^6$ kPas at 17,5°C and $\gamma_p = 5\cdot 10^{-6}~(^{\pm1})$ is applicable, also in the strain rate range 10^{-6} to $2\cdot 10^{-5}~(^{\pm1})$. Visco-elastic quantities (not presented) could be determined from back creep.

COMPUTING MODEL FOR ANALYSIS OF DEFORMATIONS

In a previous paper (Mulder, 1982) a modified version of the Bishop method of slices has been proposed as a simple tool for analysis of stability, or rather the determination of the rate of sliding of a sandasphalt-covered slope. In this method, mobilized shearing strength has been defined as:

$$\tau_s = f_s(\gamma) \tan(\phi_s)\sigma$$
 (2)

and

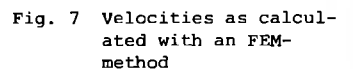
$$\tau_{a} = f_{a}(\gamma) \tan(\phi_{a})\sigma + \eta \dot{\gamma}$$
 (3)

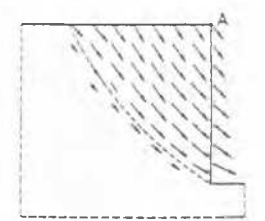
Here s and a refer to sand and sandasphalt mixture properties, γ is the time-dependent shearing strain, which is considered uniform along a potential slipcircle and σ is effective stress normal to the slipcircle. f_S and f_a are strain-dependent mobilization factors, tan (φ_S) and tan (φ_a) are internal friction parameters and η denotes the effective viscosity of the sandasphalt mixture.

When introduced into the Bishop equilibrium analysis, an ordinary differential equation for $\gamma(t)$ is obtained. The critical slip circle has been defined as the potential slip circle with either maximum limiting rate of shearing strain, or with maximum limiting value of shearing strain.

Now it is aimed to construct a simple method in order to approximately predict deformations of the slope. Therefore, consider the field of deformation rates, as calculated with a finite element method, involving an elastic ideal-plastic constitutive relation (figure 7).

The dashed line represents the critical failure arc, found by conventional equilibrium analysis.





This figure has been adopted from Ernst (1984). The pattern of displacement velocities suggests rotational sliding. It is, therefore, assumed here that the pattern of displacement of a sliding soil mass in a slope may be described as a set of concentric circular shells. The centre of rotation, associated to the shells, concides with the centre of rotation, corresponding to the critical sliding circle. Each of the shells has a different angle of rotation. The difference between angles of rotation of neighbouring shells is related to the shearing strain, or rate of shearing strain associated to the concerning slip circles, according to:

$$\gamma(t,r) = -r \frac{\partial \alpha}{\partial r} \tag{4}$$

or, equivalently:

$$\alpha(t,R) = \alpha(t,\infty) + \int_{R}^{\infty} \frac{1}{r} \gamma(t,r) dr$$
 (5)

In these equations, $\alpha(t,R)$ is the angle of rotation of the shell of radius R at time t. The strain $\gamma(t,r)$ can be obtained from (numerical) integration of the differential equation, obtained in the Bishop analysis. As a boundary condition for (5), $\alpha(t,\infty)=0$, i.e. 'infinitely' deep sliding circles are considered stable and not deformed. The procedure of construction of the field of rotations, or rates of rotations is as follows. First the critical slip circle is determined, using the modified Bishop approach. Next a set of slip circles is defined, concentric to the critical one. For each circle the strain $\gamma(t)$ is calculated, using the Bishop procedure and an incremental algorithm to solve the differential equation.

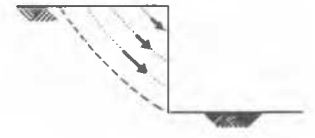


Fig. 8 Field velocities according to present analysis

Finally the field of rotation is found by discrete numerical evaluation of equation 5. Figure 8 illustrates the result of computation of the field of velocities in the case of a vertical excavation in a cohesive viscous material. For that purpose $\tan{(\varphi_a)}\sigma$ in equation 3 has been replaced by a constant C_U .

FIELD TEST (DESCRIPTION AND PREDICTION)

To observe sandasphalt behaviour in situ, a field test was set up. For that purpose two 5 m high test embankments were constructed consisting of a sand kernel with a sandasphalt overlay. On the top a vertical load of 150 kN/m' was applied in combination with a horizontal load of 40 kN/m'. After 160 days the horizontal load was increased to 80 kN/m'. The hardness of the bitumen in the sandasphalt is 80/100 (section B) and 160/210 (section A) respectively.

The mobilization function and friction angle of the sand were obtained with the standard triaxial test. For sandasphalt the test procedure described above is used.

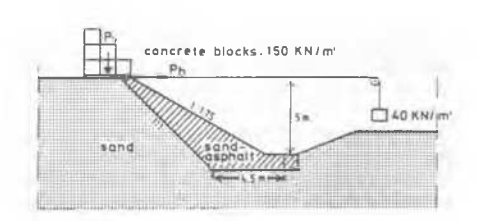


Fig. 9 Cross-section field test Schelphoek

The effective viscosity of sandasphalt depends a.o. on both the hardness of the bitumen and the density. These sensitivities have been determined with an unconfined constant load (creep) test. The results are summarized in fig. 10. In these figures the average viscosity of both sections is given.

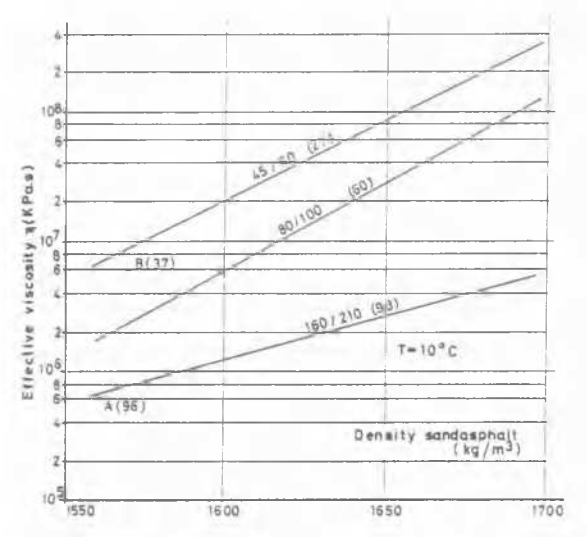


Fig. 10 Relationship between viscosity density and hardness of bitumen

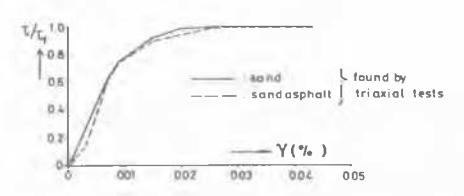


Fig. 11 Stress-strain relation of sand and sandasphalt

Predictions of the deformations and the stability have been made with above-described computing model. The results are collected in table I. The stress-strain relations used in the calculations are given in fig. 11. This table also includes the in situ measured horizontal displacements of the top of the ambankment (visualized in fig. 12). It appears that there is a considerable discrepancy between predicted and actually observed behaviour. Laboratory tests, conducted at cored samples, taken from the slope's surface after 150 days, showed a significant increase of shearing strength parameters, compared to the values found in tests at the prepared samples. Possibly due to hardening in the course of time, the angle of internal friction had increased to 39° and the viscosity had increased by a factor of 2,5 (to $1,510^7$ kPas for section B). However, in order to match calculated and measured displacements, values of 42° and 10^8 kPas should be assumed in the calculations.

CONCLUSIONS

Filter tests indicated that sandasphalt is able to withstand hydraulic gradients up to 2000 percents, without loss of permeability. This makes the material perfectly suitable for applications as a hydraulic filter. The field-test results indicate that stability and deformations behaviour is more propitious than it could be expected from theoretical analysis, based on material properties as found in laboratory tests. Further investigation is needed in order to clarify this discrepancy.

Table I: Calculated and measured deformations

	nue)	dx (continue)		dx		A	ø _B	kN/m'	kN/m'
	after days	mm/day	after	m	kPas			,	
1	10	5,0	10	0,109	102	33,5	40	40	150
11	10	7,5	10	0,151	107	13,5	36	40	150
-calculated	1n	4,0	1.0	0,088	107	33,5	44	40	150
	10	4,1	10	0,092	107	37	40	40	150
	10	6,5	10	0,111	107	30	40	40	150
	10	83,0	l n	0,831	107	33,5	4.0	80	150
section A and B		0*1	60	0,027*)		4-		40	150
B		0,25*)	5	0,044*)				80	150
A (measured	20	0.40*)	14	0.044*1				80	150

- Average found with triaxial test

^{*(}dx) plate displacement

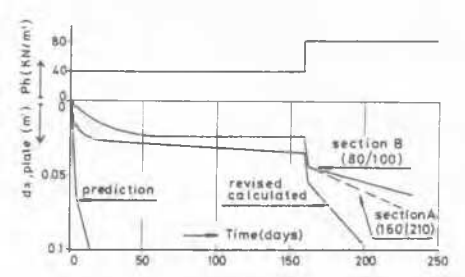


Fig. 12 Horizontal displacement of the loading plate versus time

ACKNOWLEDGEMENT

This research is supported by the Delta Dienst Rijks-waterstaat and the Centrum Onderzoek Waterkeringen. We appreciate the co-operation of co-workers of the Wegbouwkundige Dienst and the organizations mentioned.

REFERENCES

Mulder, G.; Nieuwenhuis, J.D.; Ruygrok, P.A.; Calle, E.O.F.; Petschl, R.O. (1981):

Some properties of sandasphalt in hydraulic structures - Proc. 10th Int. Conf. Soil Mech. & Found. Eng., Stockholm, Vol III, 485.

Ernst, R.J.; van Dommelen, A.E.; Vermeer, P.A. (1984): A finite element approach to slope stability (in Dutch) -P.T. Civiele & Bouwtechniek, 10 (English summary).